



Cite this: *Nanoscale*, 2018, **10**, 13410

## An electron compensation mechanism for the polymorphism of boron monolayers†

Shao-Gang Xu,<sup>‡a,b</sup> Xiao-Tian Li,<sup>‡b</sup> Yu-Jun Zhao,<sup>Ⓜb</sup> Ji-Hai Liao,<sup>b</sup> Hu Xu<sup>Ⓜ\*a</sup> and Xiao-Bao Yang<sup>Ⓜ\*b</sup>

Boron monolayers have been increasingly attractive, while it is still a challenge to understand their structural stabilities, due to electron deficiency and multi-center bonds. In this work, we propose the average electron compensation (AEC) mechanism for boron monolayers based on high-throughput first-principles calculations. It is found that the AEC parameter ( $\lambda$ ) tends to be zero for the stable free-standing boron monolayers. In addition, this mechanism can quantitatively describe the stability of boron monolayers on various metal substrates, providing direct suggestions for experimentalists to synthesize various boron monolayers for practical applications.

Received 10th February 2018,  
Accepted 16th June 2018

DOI: 10.1039/c8nr01230j

rscl.li/nanoscale

### 1. Introduction

Boron (B) clusters and monolayers have been intensively studied due to their unique properties arising from structural diversity. Different from the bulk structure<sup>1</sup> consisting of B<sub>12</sub>-icosahedra,<sup>2</sup> various planar or quasi-planar B<sub>n</sub> clusters received a great deal of theoretical and experimental attention in recent years.<sup>3–7</sup> For example, B<sub>38</sub> with a double-hexagonal vacancy was initially predicted theoretically in 2015,<sup>6</sup> and it was successfully confirmed by photoelectron spectra measurements in 2017.<sup>7</sup> Boron monolayers with hexagonal vacancies were theoretically proposed around a decade ago,<sup>8,9</sup> followed by extensive studies that demonstrated that the stable, flat and free-standing boron monolayers would exhibit rich polymorphism within a narrow range of energies,<sup>10,11</sup> as well as the corresponding hexagonal vacancy concentration  $\eta$  in the range of  $1/9 \leq \eta \leq 1/7$ .<sup>8,10,12,13</sup>

The charge transfer between boron monolayers and metal substrates will greatly alter the structural stability of boron monolayers. Excitingly, the  $\beta_{12}$  ( $\eta = 1/6$ ) and  $\chi_3$  ( $\eta = 1/5$ ) sheets have been recently synthesized on the Ag (111) substrate,<sup>14,15</sup> while first-principles calculations<sup>16,17</sup> suggested that the free-standing  $\beta_{12}$  and  $\chi_3$  sheets are not stable. Boron monolayers deposited on metal substrates are very sensitive to growth conditions,<sup>11,18,19</sup> and various metastable phases of boron mono-

layers including the famous  $\alpha$  sheet were observed by molecular beam epitaxy (MBE) experiments.<sup>18,20</sup> In addition, the adjustable interaction of metal substrates with the polymeric boron monolayers may lead to various promising applications in catalyst reactions,<sup>21</sup> Li-ion batteries,<sup>22</sup> and hydrogen storage.<sup>23,24</sup>

The concentration and distribution of hexagonal vacancies dominate the stability of boron monolayers. However, a quantitative model is still absent to describe their stability due to complicated bonding. In this work, we propose the average electron compensation (AEC) model for the stability of boron monolayers, where the possible candidates are enumerated based on first-principles calculations with the congruence check. The calculated AEC parameter ( $\lambda$ ) of the stable free-standing boron monolayer is found to be near zero, while the electron-deficient boron monolayers with larger  $\lambda$  are more stable on metal substrates as verified by first-principles calculations.

### 2. Computational details

The first-principles calculations were performed based on density functional theory (DFT) as implemented in the Vienna *ab initio* simulation package (VASP).<sup>25</sup> The electron-ion interactions were described by the projector augmented wave (PAW) method.<sup>26</sup> To treat the exchange–correlation interaction of electrons, we chose the Perdew–Burke–Ernzerhof (PBE) functional within the generalized gradient approximation (GGA).<sup>27</sup> The energy cutoff was set to 480 eV, and the forces acting on each atom were less than 0.01 eV Å<sup>-1</sup>. To investigate the dynamic and thermal stability of boron monolayers, we calculated phonon dispersion using the Phonopy package<sup>28</sup> and

<sup>a</sup>Department of Physics, Southern University of Science and Technology, Shenzhen 518055, P. R. China. E-mail: xuh@sustc.edu.cn

<sup>b</sup>Department of Physics, South China University of Technology, Guangzhou 510640, P. R. China. E-mail: scxbyang@scut.edu.cn

†Electronic supplementary information (ESI) available. See DOI: 10.1039/c8nr01230j

‡These authors contributed equally to this work.

carried out *ab initio* molecular dynamics (AIMD) simulations with a Nosé–Hoover thermostat<sup>29</sup> at various temperatures. In addition, we employed more accurate hybrid functional calculations (HSE06 and PBE0)<sup>30–32</sup> to confirm the relative stability of the boron monolayers with lower energies.

Based on the triangular lattice supercell with various hexagonal vacancy distributions, we have enumerated the possible candidates with the number of atoms in the cell less than 30. The average formation energy ( $E_{\text{form}}$ ) of the B sheets is defined as  $E_{\text{form}} = (E_{\text{sheet}}/n - E_{\text{at}})$ , where  $E_{\text{sheet}}$  is the total energy of the B sheet,  $E_{\text{at}}$  is the energy of an isolated spin-polarized boron atom, and  $n$  is the number of B atoms in the cell. The average adsorption (formation) energies for boron monolayers on the metal substrates are defined in the ESI.† The removal of one boron atom from the flat triangular sheet produces a hexagonal vacancy, generating a mixture of hexagons and triangles, and  $\eta$  is defined as<sup>8</sup>

$$\eta = \frac{\text{No. of hexagonal vacancies}}{\text{No. of atoms in the original triangular sheet}}$$

The charge difference of boron sheets is defined as:  $\Delta\rho = \rho(\text{B}_2) - \rho(\text{B}_1)$ , where  $\rho(\text{B}_2)$  refers to the charge densities of the boron sheets from self-consistent calculation, and  $\rho(\text{B}_1)$  is the summation of free atomic charge densities for the boron sheets. For the adsorption systems, the charge difference is defined as:  $\Delta\rho = \rho(\text{Sub} + \text{Bsheet}) - \rho(\text{Sub}) - \rho(\text{Bsheet})$ , where  $\rho(\text{Sub} + \text{Bsheet})$  is the charge densities of the B/Ag systems and  $\rho(\text{Sub})$  and  $\rho(\text{Bsheet})$  are the charge densities for isolated systems.

## 3. Results and discussion

### 3.1 Structural stability of boron monolayers

Boron monolayers with a high vacancy concentration ( $\eta \geq 6/27$ ) tend to become amorphous,<sup>33</sup> and therefore in this work we focus on the structures in the vacancy concentration of  $1/12 \leq \eta$

$\leq 1/5$  to maintain the stabilities. As shown in Fig. 1a, the convex hull dots represent the ground-state boron monolayers as a function of  $\eta$ , and the corresponding structures are presented in Fig. 1b. Instead of cluster expansion (CE) and particle-swarm optimization (PSO),<sup>12,13</sup> we have performed a full screening of possible boron monolayers from the triangular lattice with hexagonal vacancies, using the structure recognition algorithm based on distance matrices proposed by our group.<sup>34,35</sup> All the stable phases in the previous literature<sup>8,10,12,13</sup> were found in our enumerated calculations. In addition, we uncovered more stable boron monolayers with  $\eta$  of 1/10 (−5.948 eV per atom), 1/6 (−5.970 eV per atom) and 5/28 (−5.957 eV per atom) for the first time, compared to those found in the earlier studies.<sup>13</sup> Note that the coordination number (CN) of B atoms of the stable candidates is not smaller than 4, and thus the candidates with CN = 3 are excluded to accelerate the screening efficiency (shown in Fig. 1a).

The representative free-standing boron monolayers with lower energies reported in the literature<sup>8,10,12,36,37</sup> are listed in Table S2.† In addition, we find a stable boron monolayer with a novel armchair hexagonal-vacancy chain ( $\beta_{\text{arm}}$ ) (shown in Fig. S1a†). According to the phonon dispersion and AIMD simulations (shown in Fig. S1†), we show that  $\beta_{\text{arm}}$  has outstanding dynamic and thermal stabilities. Furthermore, the accurate hybrid functional calculations also confirm that boron monolayers with  $\eta_{4/28}$  and  $\eta_{1/8}$  are the most stable, where the energy differences between these stable phases are less than 10 meV per atom (shown in Table S2†). Although the results from hybrid functional calculations may slightly change the energy difference between the structures, they will not qualitatively affect the conclusions, indicating the polymorphism of the ground-state boron sheets.

### 3.2 Electronic properties and bonding analysis of boron monolayers

We have calculated the projected density of states (PDOS) for some boron monolayers with the separated in-plane (the sum

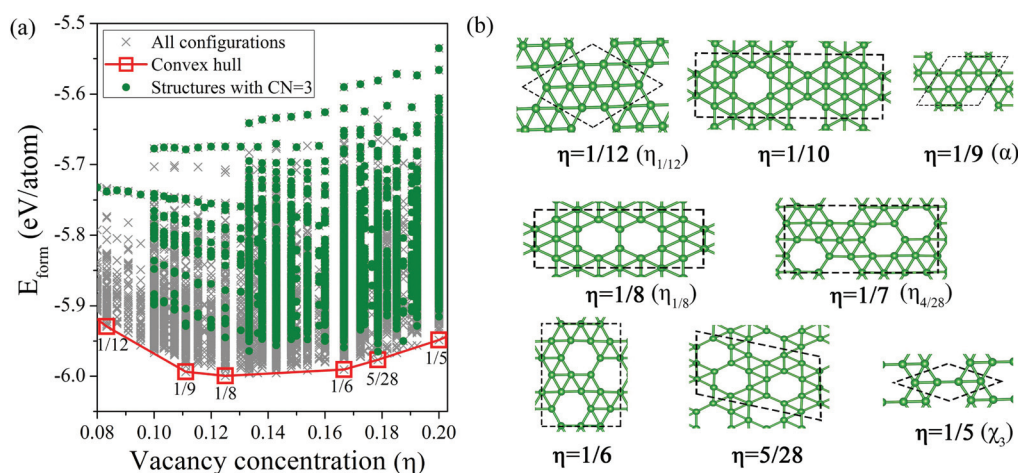


**Fig. 1** (a) The average formation energies  $E_{\text{form}}$  as a function of the vacancy concentration  $\eta$  for the boron monolayers, and the green dots represent the candidates with a coordination number (CN) of 3. (b) The atomic structures of the most stable boron monolayers at fixed  $\eta$ . The energies in (a) are based on the PBE functional calculations.

of  $s$ ,  $p_x$  and  $p_y$ )  $s + p_{x,y}$  orbitals and out-of-plane  $p_z$  orbitals shown in Fig. S2.† All the low-lying boron monolayers at various  $\eta$  are metallic characterized by the  $p_z$ -derived bands, where the Fermi level ( $E_F$ ) lying in the gap of the in-plane bonding and anti-bonding states for most stable boron monolayers represents the good balance of the triangular regions (donors) and hexagonal regions (acceptors).<sup>8,10</sup> However, the stabilizing mechanism remains a subject of debate, since there are a few unstable boron monolayers with  $\eta > 1/7$  in which the  $E_F$  is located in the gap of the in-plane orbitals (see Fig. S3†). In addition, the PDOS analysis shouldn't be employed to screen stable structures, since it cannot be obtained without the first-principles calculations.

To explain the structural stability and charge distribution of boron clusters, we have proposed an effective 8-electron model<sup>6</sup> based on two main assumptions: (i) there are  $3n$  ( $n$  is the number of boron atoms in a unit cell) valence electrons to form  $2c-2e$  (single-bond) bonds and  $3c-2e$  (three-center bond) bonds. In order to ensure that each B atom satisfies the 8-electron rule, we have  $\sum_{i=1}^{m_1} 2s_i + \sum_{j=1}^{m_2} 2t_j = 3n$  and  $\sum_{i=1}^{m_1} 4s_i + \sum_{j=1}^{m_2} 6t_j = 8n$ , where  $m_1(m_2)$  represents the number of all the  $2c-2e$  ( $3c-2e$ ) bonds and the occupations (*i.e.*,  $s_i$ ,  $t_j$ ) of  $2c-2e$  ( $3c-2e$ ) bonds are in the range from 0 to 1; and (ii) the distribution of  $2c-2e$  and  $3c-2e$  bonds should be in agreement with the charge difference and the symmetry of the configuration. Based on the 8-electron rule, the boron cluster candidates can be pre-screened qualitatively by the geometry.<sup>38</sup>

To understand the stability of boron monolayers, we herein propose a quantitative AEC model. Similar to the former 8-electron model, the  $3c-2e$  bonds are located at the triangle regions and the  $2c-2e$  bonds are located at the edges of hexagons, respectively, where " $s_i$ " and " $t_j$ " are the occupation numbers of the  $i$ -th  $2c-2e$  and  $j$ -th  $3c-2e$  bonds. The matrices for the given boron sheets are based on two basic principles: (i) the electron number of all the  $2c-2e$  and  $3c-2e$  bonds equals  $(3 + \lambda) \times n$ , as the total valence electron number in the unit cell is  $3 \times n$ ,  $\lambda$  represents the average electron compensation parameter; and (ii) the distributions of the  $2c-2e$  ( $3c-2e$ ) bond ensure that every B atom in the unit cell satisfies the 8-electron rule. Each  $2c-2e$  ( $3c-2e$ ) bond shares 2 electrons with two (three) B atoms, thus the total number of bonds for each B atom is 4 to satisfy the 8-electron rule, with the bond occupation number ( $s_i$ ,  $t_j$ ) in the range of (0–1). Under this definition, boron monolayers with positive  $\lambda$  are electron deficient.

Here we may apply the AEC model to analyze the experimentally synthesized boron monolayers ( $\chi_3$ ,  $\beta_{12}$ ),<sup>15</sup> as shown in Fig. 2(a and b). Considering the symmetry of the structure, we determine the inequivalent  $2c-2e$  bonds and  $3c-2e$  bonds in the unit cell. Taking the  $\chi_3$  sheet as an example, there are two inequivalent atoms (marked by various colors) in the unit cell, corresponding to one inequivalent  $3c-2e$  bond ( $t_1$ ) and two inequivalent  $2c-2e$  bonds ( $s_1$ ,  $s_2$ ). Considering the number of valence electrons, we have  $8s_1 + 2s_2 + 8t_1 = (3 + \lambda) \times 4$ . For the

two atoms, we have  $2s_1 + 4t_1 = 4$  and  $2s_1 + s_2 + 2t_1 = 4$  to satisfy the 8-electron rule, where the corresponding matrix ( $A$ ) is obtained (shown in Fig. 2a), and we find a unique  $\lambda$  of 0.5 for the  $\chi_3$  sheet. The full process contains two steps: (i) writing a linear equation ( $A \times X^T = B$ ) for the given boron sheet candidate; and (ii) applying a numerical algorithm to find the  $\lambda$  with the minimum absolute value to ensure that the solutions " $X$ " are located in the range of 0 and 1. The  $\beta_{12}$  sheet is also checked in a similar way as shown in Fig. 2b. The AEC model analysis results for other typical boron monolayers are presented in Table S3.† The AEC parameter of the  $\eta_{2/15}$  sheet is calculated to be 0.077 e per atom, which is in agreement with the recent theoretical work<sup>39</sup> where the ground-state boron monolayer is the  $\eta_{2/15}$  sheet at a low charge doping level ( $q = 0.03$  e per atom).

According to the relationship of the average formation energy and AEC parameter (shown in Fig. 2c), the boron monolayers with  $\eta < 1/9$  are proved to be electron-excessive with negative  $\lambda$ , while the free-standing unstable boron monolayers ( $\beta_{12}$  and  $\chi_3$ )<sup>15</sup> are found to be electron deficient due to the relative large  $\lambda$ . It is worth noting that, all the stable boron monolayers correspond to a smaller  $\lambda$  ( $0 \leq \lambda < 0.08$ ), because the stable boron monolayers should not be electron-excessive (negative  $\lambda$ ) with the occupation of anti-bonding states, and the boron monolayers with a large  $\lambda$  should be seriously electron deficient.

As shown in Fig. S4,† there are lots of candidates with a given  $\eta$ , and the structural stabilities cannot be pre-judged without performing the first-principles calculations. In our AEC model, the descriptor  $\lambda$  proves that the best value for stable boron monolayers is close to zero, and adopting a reasonable constraint ( $\lambda = 0$ ) can help us screen the stable boron monolayers based on the geometry instead of the first-principles calculations. The self-doping mechanism in earlier works<sup>40,41</sup> successfully analyzed the chemical bonding of the given boron monolayers from maximally localized Wannier functions.<sup>42</sup> The method, however, is expensive to screen numerous candidates since it is based on first-principles calculations.

In our previous studies,<sup>6,38</sup> we adopted the 8-electron rule with a fractional solution to analyze the bond distribution of the magic boron clusters, which should also be in agreement with the charge difference. In Fig. 3, we show the charge difference of the four stable boron monolayers, where the warm/cold color regions represent the electron localization and the electron deficiency, respectively. Using our AEC model, we find a possible discrete occupation number of 1/4 for the  $2c-2e$  and  $3c-2e$  bond to analyze the most stable  $\eta_{4/28}$  sheet ( $\lambda = 0$ ). As shown in Fig. 3a, there are {12, 8, 12}  $3c-2e$  bonds with the occupation number of {1/2, 3/4, 1} and {8, 4, 8, 2}  $2c-2e$  bonds with the occupation number of {1/4, 1/2, 3/4, 1}. Fig. 3b shows the charge difference and model analysis of  $2c-2e$  and  $3c-2e$  bond distributions for the  $\eta_{1/8}$  sheet with a unique  $\lambda$  of 0.048. There are 20 (12) bonds of  $3c-2e$  ( $2c-2e$ ) with the occupation of 3/4, 10 (4) bonds of  $3c-2e$  ( $2c-2e$ ) with the occupation of 1/2, and only 1 bond of  $2c-2e$  at the center with the occupation of

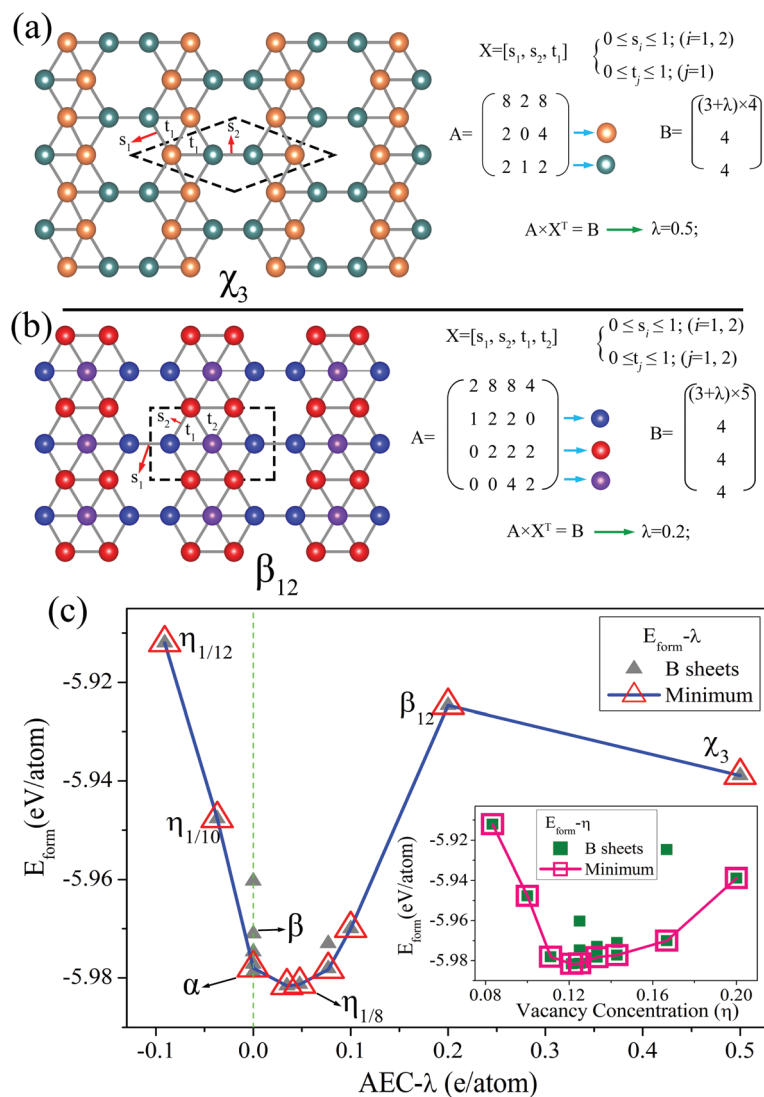


**Fig. 2** (a, b) AEC model analysis for  $\chi_3$  and  $\beta_{12}$ , the black dashed lines represent the unit cell of the boron monolayers, and the atoms with various colors represent the inequivalent atoms. Note that “ $s_i$ ” and “ $t_j$ ” are the occupation numbers of  $i$ -th 2c-2e (single-bond) and  $j$ -th 3c-2e (three-center bond) bonds at the edges and triangles, respectively. (c) The formation energies  $E_{\text{form}}$  as a function of the AEC parameter  $\lambda$  for several boron monolayers with  $1/12 \leq \eta \leq 1/5$ . The inset represents  $E_{\text{form}}$  as a function of  $\eta$ . The energy data in (c) are based on PBE functional calculations.

1. In particular, the B–B bond length (1.64 Å) of the edge connecting the two hexagons is shorter than the one (1.69 Å) belonging to an independent hexagon, and our model solution can present the electron localization in the region with a maximum occupation number of 1 for the 2c-2e bond.

For the first proposed stable boron monolayer ( $\alpha$  sheet),<sup>8,9</sup> our model can also give a reasonable solution with the minimum occupation number of 1/3 with  $\lambda = 0$ . As shown in Fig. 3c, the bond distributions contain {6, 6} 3c-2e bonds with the occupations of {1, 1/3}, and 6 2c-2e bonds with the occupation of 2/3. Insight into the charge difference of the  $\alpha$  sheet revealed that all the hexagonal edges in the unit cell are equivalent, in agreement with our model solution. For the new predicted flat phase  $\beta_{\text{arm}}$  (shown in Fig. 3d), there are 24 (12) bonds of 3c-2e (2c-2e) with the occupation of 3/4, 12 (6) bonds

of 3c-2e (2c-2e) with the occupation of 1/2, and 4 bonds of 2c-2e with the occupation of 1 (the intact 2c-2e bonds reflect the electron localization in the armchair regions). Other stable boron monolayers can also be analyzed by our model with the minimum occupation of 1/2 for the 2c-2e and 3c-2e bonds (shown in Fig. S5†), indicating that our model is an effective and universal method to analyze the electron distributions in the stable boron monolayers with a clear and simple picture.

### 3.3 The interaction of boron monolayers with metal substrates

To investigate the possibility of boron monolayers fabricated in the experiments, we have systematically studied the structural stability of several boron monolayers placed on the Ag substrate (shown in Fig. S6†). Fig. 4a shows the stabilities of

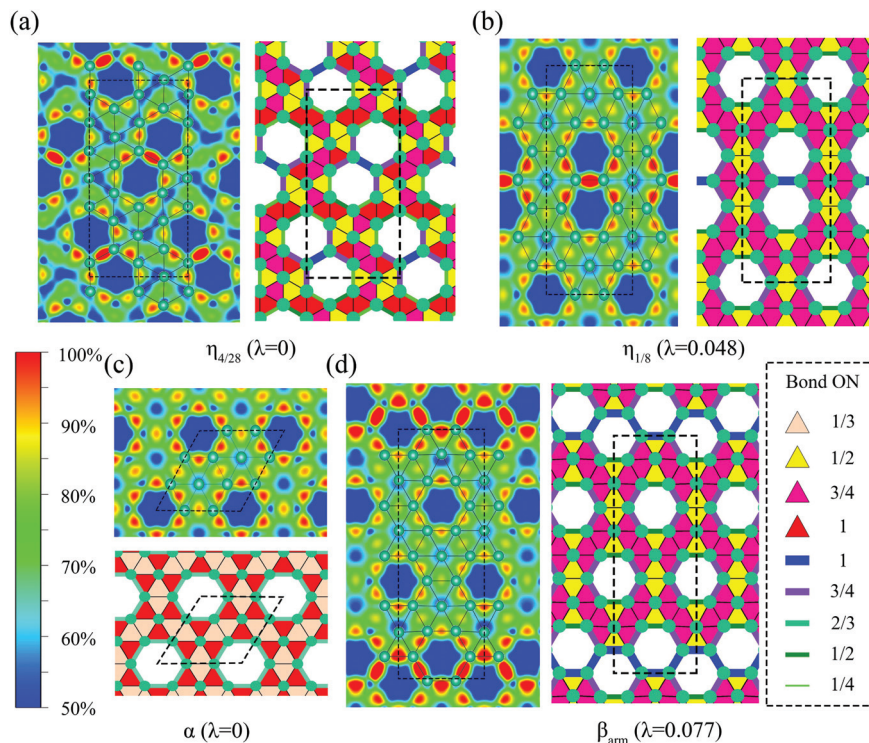


**Fig. 3** Bonding analysis for a few stable boron monolayers. The left part of (a–d) showed the charge difference of the corresponding boron monolayers, and the right part of (a–d) showed the possible 2c-2e and 3c-2e bond distributions. The percentages of the color bar are signed with the peak amplitude value for the isosurface located at the left side of the figure and the occupation numbers (ON) of the 2c-2e and 3c-2e bonds are listed on the right side of the figure. The above charge differences are calculated using the PBE functional.

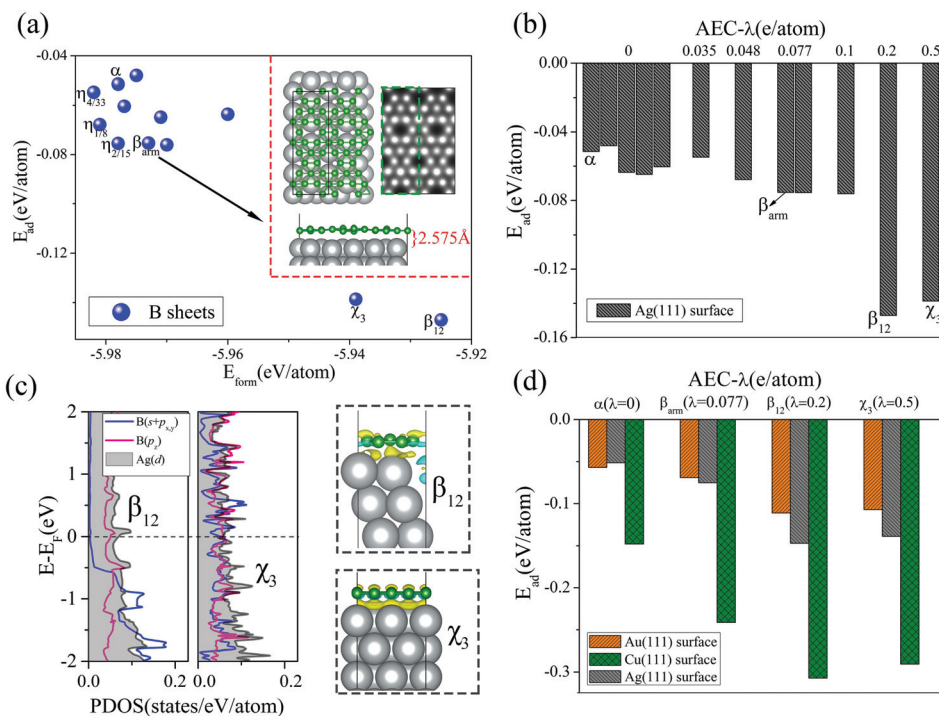


**Fig. 4** (a) The relationship of  $E_{\text{ad}}$  and  $E_{\text{form}}$  for the boron monolayers; the inset represents the top and side view of the  $\beta_{\text{arm}}$  monolayer on the Ag (111) surface and the corresponding simulated STM image. (b) The relationship of  $E_{\text{ad}}$  and the AEC parameter  $\lambda$  for the B/Ag systems. (c) PDOS analysis and charge difference for the  $\beta_{12}$  and  $\chi_3$  monolayers on the metal substrates. (d) The average adsorption energy of the four typical boron monolayers on the Au/Cu/Ag (111) surfaces. All the data in this figure are calculated using the PBE functional.

boron monolayers ( $\eta_{4/33}$ ,  $\eta_{1/8}$ ,  $\eta_{2/15}$ ,  $\beta_{\text{arm}}$ , etc.) that might be fabricated on the Ag substrate under proper conditions, since these monolayers are more stable than the  $\alpha$  sheet that has been synthesized.<sup>20</sup> The average formation energy ( $E_{\text{form}}$ ) of the stable free-standing  $\beta_{\text{arm}}$  and  $\eta_{2/15}$  on the Ag (111) substrate is only 0.02 eV per atom higher than those of the experimental ( $\beta_{12}$ ,  $\chi_3$ ) sheets, and the overall stability of the boron monolayers on the Ag (111) substrate is shown in Fig. S7.† The average adsorption energies ( $E_{\text{ad}}$ ) (shown in Fig. 4b) are lower for these boron monolayers with larger  $\lambda$ , indicating a stronger interaction with the Ag substrate due to a greater charge transfer.<sup>11,33</sup> According to the PDOS analysis for the  $\beta_{12}$  and  $\chi_3$  monolayers (shown in Fig. 4c), both the out-of-plane  $p_z$  and in-plane  $s + p_{x,y}$  orbitals participate in hybridizing with the Ag 4d orbitals, and the charge differences indicate a strong interaction of the boron monolayers with the Ag substrate.

While different metal substrates may alter the ground-state structures of 2D B due to the various abilities of charge transfer, we also consider four typical boron monolayers on the Au/Cu substrates, which would not form borides,<sup>33</sup> as shown in Fig. S8.† The adsorption energy on the Au substrate is similar to that on the Ag substrate, and a much stronger interaction occurs on the Cu substrate, which can be confirmed from the relative distance of boron monolayers and metal substrates. For the new predicted stable  $\beta_{\text{arm}}$  with ( $\lambda = 0.077$ ), the stronger  $E_{\text{ad}}$  than that of the  $\alpha$  sheet may be attributed to the local environments of the armchair regions with low atomic concentration. The trends of the average adsorption energy and  $\lambda$  (Fig. 4d) show that, the boron monolayers with a larger  $\lambda$  correspond to a stronger interaction with metal substrates, indicating the rationality of our AEC model. The former theoretical results<sup>37</sup> indicate that the adhesive energy of silicene on the Ag (111) substrate is much stronger than that of the  $\beta_{12}$  sheet on Ag/Au/Cu (111) substrates, and the exfoliation of silicene from the Ag (111) substrate has been reported in experiments.<sup>43</sup> Despite the difficulties, many theoretical and experimental efforts have been devoted to study this issue, and we believe that the 2D B sheets will be separated from the substrates by a special process in the future. Recently, the graphene-like borophene has been synthesized on the Al (111) surface.<sup>44</sup> The free-standing honeycomb is unstable due to the heavy electron deficiency, and nearly one electron charge is transferred to each boron atom from the Al (111) substrate to stabilize the honeycomb borophene.<sup>44,45</sup> We are inclined to believe that, various boron monolayers may be synthesized by the control of growth conditions in the future.

## 4. Conclusions

In summary, we have systematically investigated the possible boron monolayers based on high-throughput screening with first-principles calculations, where a novel stable boron monolayer  $\beta_{\text{arm}}$  with armchair hexagonal-vacancy chains is obtained. The AEC model is proposed to describe the electron deficiency in boron monolayers quantitatively, providing an excellent

explanation of the stability evolutions for boron monolayers as a function of substrates. Our findings give a valuable insight to help us understand the intriguing electronic properties of boron monolayers. Notably, the boron monolayer  $\beta_{\text{arm}}$  would be stable with/without substrates, exhibiting its potential in practical applications.

## Conflicts of interest

There are no conflicts of interest to declare.

## Acknowledgements

This work was supported by the National Natural Science Foundation of China (No. 11474100, 11674148, 11574088), the Guangdong Natural Science Funds for Distinguished Young Scholars (No. 2014A030306024, 2017B030306008), the Basic Research Program of Science, Technology and Innovation Commission of Shenzhen Municipality (Grant No. JCYJ20160531190054083), and the Guangdong Natural Science Funds for Doctoral Program (Grant No. 2017A030310086). The computer times at the National Supercomputing Center in Guangzhou (NSCCGZ) and Guangzhou Ginpie Technology are gratefully acknowledged.

## References

- 1 B. Albert and H. Hillebrecht, *Angew. Chem., Int. Ed.*, 2009, **48**, 8640–8668.
- 2 M. Fujimori, T. Nakata, T. Nakayama, E. Nishibori, K. Kimura, M. Takata and M. Sakata, *Phys. Rev. Lett.*, 1999, **82**, 4452–4455.
- 3 W. L. Li, Y. F. Zhao, H. S. Hu, J. Li and L. S. Wang, *Angew. Chem., Int. Ed.*, 2014, **53**, 5540–5545.
- 4 W. L. Li, Q. Chen, W. J. Tian, H. Bai, Y. F. Zhao, H. S. Hu, J. Li, H. J. Zhai, S. D. Li and L. S. Wang, *J. Am. Chem. Soc.*, 2014, **136**, 12257–12260.
- 5 Z. A. Piazza, H. S. Hu, W. L. Li, Y. F. Zhao, J. Li and L. S. Wang, *Nat. Commun.*, 2014, **5**, 3113.
- 6 S.-G. Xu, Y.-J. Zhao, J.-H. Liao and X.-B. Yang, *J. Chem. Phys.*, 2015, **142**, 214307.
- 7 Q. Chen, W.-J. Tian, L.-Y. Feng, H.-G. Lu, Y.-W. Mu, H.-J. Zhai, S.-D. Li and L.-S. Wang, *Nanoscale*, 2017, **9**, 4550–4557.
- 8 H. Tang and S. Ismail-Beigi, *Phys. Rev. Lett.*, 2007, **99**, 115501.
- 9 X. Yang, Y. Ding and J. Ni, *Phys. Rev. B: Condens. Matter Mater. Phys.*, 2008, **77**, 041402.
- 10 E. S. Penev, S. Bhowmick, A. Sadrzadeh and B. I. Yakobson, *Nano Lett.*, 2012, **12**, 2441–2445.
- 11 Z. Zhang, E. S. Penev and B. I. Yakobson, *Nat. Chem.*, 2016, **8**, 525–527.
- 12 X. Wu, J. Dai, Y. Zhao, Z. Zhuo, J. Yang and X. C. Zeng, *ACS Nano*, 2012, **6**, 7443–7453.

- 13 X. Yu, L. Li, X.-W. Xu and C.-C. Tang, *J. Phys. Chem. C*, 2012, **116**, 20075–20079.
- 14 A. J. Mannix, X.-F. Zhou, B. Kiraly, J. D. Wood, D. Alducin, B. D. Myers, X. Liu, B. L. Fisher, U. Santiago, J. R. Guest, M. J. Yacaman, A. Ponce, A. R. Oganov, M. C. Hersam and N. P. Guisinger, *Science*, 2015, **350**, 1513–1516.
- 15 B. J. Feng, J. Zhang, Q. Zhong, W. B. Li, S. Li, H. Li, P. Cheng, S. Meng, L. Chen and K. H. Wu, *Nat. Chem.*, 2016, **8**, 564–569.
- 16 S. G. Xu, Y. J. Zhao, J. H. Liao, X. B. Yang and H. Xu, *Nano Res.*, 2016, **9**, 2616–2622.
- 17 H. Shu, F. Li, P. Liang and X. Chen, *Nanoscale*, 2016, **8**, 16284–16291.
- 18 Z. Zhang, A. J. Mannix, Z. Hu, B. Kiraly, N. P. Guisinger, M. C. Hersam and B. I. Yakobson, *Nano Lett.*, 2016, **16**, 6622–6627.
- 19 N. Karmodak and E. D. Jemmis, *Angew. Chem., Int. Ed.*, 2017, **56**, 10093–10097.
- 20 Z. Qing, Z. Jin, C. Peng, F. Baojie, L. Wenbin, S. Shaoxiang, L. Hui, M. Sheng, C. Lan and W. Kehui, *J. Phys.: Condens. Matter*, 2017, **29**, 095002.
- 21 C. Ling, L. Shi, Y. Ouyang, X. C. Zeng and J. Wang, *Nano Lett.*, 2017, **17**, 5133–5139.
- 22 X. Zhang, J. Hu, Y. Cheng, H. Y. Yang, Y. Yao and S. A. Yang, *Nanoscale*, 2016, **8**, 15340–15347.
- 23 S. Er, G. A. de Wijs and G. Brocks, *J. Phys. Chem. C*, 2009, **113**, 18962–18967.
- 24 J. Li, H. Zhang and G. Yang, *J. Phys. Chem. C*, 2015, **119**, 19681–19688.
- 25 G. Kresse and J. Furthmüller, *Phys. Rev. B: Condens. Matter Mater. Phys.*, 1996, **54**, 11169–11186.
- 26 G. Kresse and D. Joubert, *Phys. Rev. B: Condens. Matter Mater. Phys.*, 1999, **59**, 1758–1775.
- 27 J. P. Perdew, K. Burke and M. Ernzerhof, *Phys. Rev. Lett.*, 1996, **77**, 3865–3868.
- 28 A. Togo, F. Oba and I. Tanaka, *Phys. Rev. B: Condens. Matter Mater. Phys.*, 2008, **78**, 134106.
- 29 S. Nosé, *J. Chem. Phys.*, 1984, **81**, 511–519.
- 30 J. Heyd, G. E. Scuseria and M. Ernzerhof, *J. Chem. Phys.*, 2003, **118**, 8207–8215.
- 31 J. Paier, M. Marsman, K. Hummer, G. Kresse, I. C. Gerber and J. G. Ángyán, *J. Chem. Phys.*, 2006, **124**, 154709.
- 32 J. P. Perdew, M. Ernzerhof and K. Burke, *J. Chem. Phys.*, 1996, **105**, 9982–9985.
- 33 Y. Liu, E. S. Penev and B. I. Yakobson, *Angew. Chem., Int. Ed.*, 2013, **52**, 3156–3159.
- 34 X.-T. Li, S.-G. Xu, X.-B. Yang and Y.-J. Zhao, *J. Chem. Phys.*, 2017, **147**, 144106.
- 35 X.-T. Li, X.-B. Yang and Y.-J. Zhao, *J. Chem. Phys.*, 2017, **146**, 154108.
- 36 H. Lu, Y. Mu, H. Bai, Q. Chen and S. D. Li, *J. Chem. Phys.*, 2013, **138**, 024701.
- 37 Z. Zhang, Y. Yang, G. Gao and B. I. Yakobson, *Angew. Chem., Int. Ed.*, 2015, **53**, 13022–13026.
- 38 S.-G. Xu, Y.-J. Zhao, X.-B. Yang and H. Xu, *J. Phys. Chem. C*, 2017, **121**, 11950–11955.
- 39 Z. Zhang, S. N. Shirodkar, Y. Yang and B. I. Yakobson, *Angew. Chem., Int. Ed.*, 2017, **56**, 15421–15426.
- 40 H. Tang and S. Ismail-Beigi, *Phys. Rev. B: Condens. Matter Mater. Phys.*, 2009, **80**, 134113.
- 41 C.-C. Lee, B. Feng, M. D'Angelo, R. Yukawa, R.-Y. Liu, T. Kondo, H. Kumigashira, I. Matsuda and T. Ozaki, *Phys. Rev. B: Condens. Matter Mater. Phys.*, 2018, **97**, 075430.
- 42 N. Marzari, A. A. Mostofi, J. R. Yates, I. Souza and D. Vanderbilt, *Rev. Mod. Phys.*, 2012, **84**, 1419–1475.
- 43 L. Tao, E. Cinquanta, D. Chiappe, C. Grazianetti, M. Fanciulli, M. Dubey, A. Molle and D. Akinwande, *Nat. Nanotechnol.*, 2015, **10**, 227.
- 44 W. Li, L. Kong, C. Chen, J. Gou, S. Sheng, W. Zhang, H. Li, L. Chen, P. Cheng and K. Wu, *Sci. Bull.*, 2018, **63**, 282–286.
- 45 S. N. Shirodkar, E. S. Penev and B. I. Yakobson, *Sci. Bull.*, 2018, **63**, 270–271.